Planar defects in ZnO thin films deposited on optical fibers and flat substrates

Laurent Sagalowicz[a)] and Glen R. Fox[b)]
Laboratoire de Céramique, Département des Matériaux, EPFL, 1015 Lausanne, Switzerland

The microstructure and the defects of ZnO coatings deposited at room temperature by sputtering onto fibers and flat substrates were characterized using transmission electron microscopy (TEM), scanning electron microscopy, and x-ray diffraction (XRD). XRD shows that the films have a [0001] preferred orientation and a large angular width of the 0002 reflection. According to TEM observations, the film microstructure consists of columnar grains which contain large concentrations of basal planar defects and dislocations. High-resolution transmission electron microscopy analysis and the associated image simulation are in full agreement with the presence of single (type I) and double (type II) stacking faults. The relation between the observed defects and the 0002 peak broadening is discussed.

I. INTRODUCTION

ZnO thin films have been studied for a wide variety of applications including piezoelectric surface acoustic wave devices,[1,2] varistors,[3–5] optical waveguides,[6] transparent electrodes,[7] and gas sensors.[8] In addition, ZnO coatings deposited on optical fibers show promise for the development of new active all-fiber devices including phase modulators,[9,10] wavelength modulators,[11] electric field sensors,[12,13] and flexural actuators.[14] It is well established that the microstructure, in particular the [0001] preferred orientation, of ZnO thin films strongly influences both electrical and optical properties. In fact, ZnO thin films cannot be used for certain applications, e.g., piezoelectric sensors and actuators, unless they exhibit a preferred orientation, which is commonly [0001] perpendicular to the substrate plane for films deposited by sputtering.[6,15] In this article, the microstructures of [0001] textured ZnO thin films deposited onto flat and fiber substrates are analyzed from the atomic to the micron scale in order to give more insight into which microstructural features are present that can influence thin film properties.

ZnO thin films deposited by sputter deposition methods tend to exhibit columnar microstructures for a relatively broad range of deposition conditions. The occurrence of these columnar microstructures has been confirmed by several studies that have employed scanning electron microscopy (SEM).[16–19]

X-ray diffraction (XRD) has been used to determine that the columnar grains tend to exhibit a preferred orientation with the [0001] direction perpendicular to the plane of a planar substrate. The standard deviation of the x-ray diffraction rocking curve of the 0002 diffraction peak ($\sigma 0002$) is commonly used to characterize the degree of [0001] texture, which is dependent on deposition conditions and the substrate material.[20–23] XRD has also been used to identify the existence of defects within the lattice of the columnar ZnO grains. Several authors have noted that the angular width of the 0002 reflection (B_{0002}) is dependent upon processing conditions including deposition rate, pressure, and temperature.[17,22,24,25] The broadening of the 0002 peak is generally attributed to the occurrence of a small "crystallite" size of less than 100 nm along the [0001] direction, but this conclusion provides only a vague explanation for the observed peak broadening and the exact nature of the "crystallites" and defects is not known.[26] In fact, broadening of a diffraction peak can result from the occurrence of several types of perturbations of the crystalline lattice including nonuniform strain, planar defects, dislocations, and grain boundaries.[27]

In this study, transmission electron microscopy (TEM) was used to give a detailed description of the defects and microstructure which may be responsible for the XRD 0002 peak broadening. TEM observations of undoped ZnO powders and ceramics that were heated to temperatures below 900 °C have shown the existence of stacking faults[28,29] in the (0001) basal plane in combination with partial dislocations. Samples heated above 1000 °C do not exhibit stacking faults, indicating that the occurrence of these faults is dependent upon the thermal history of the ZnO.[29] The ZnO (space group $P6_3mc$, $a = 0.3253$ nm, $c = 0.5213$ nm, and $u = 0.382$) has a wurtzite structure, which is based on a hexagonal Bravais lattice. The oxygen stacking is similar to an hcp structure, and the cations occupy one-half of the tetrahedral sites. The stacking sequence along [0001] of the

[a)]e-mail: laurent.sagalowicz@epfl.ch
[b)]Present address: Ramtron International Corporation, 1850 Ramtron Drive, Colorado Springs, Colorado 80921.

wurtzite structure may be described as AaBbAaB...
where the capital letters designate oxygen atoms and the
small letters designate Zn atoms. Locally the hexagonal
arrangement may transform to a sphalerite (cubic)
structure giving rise to one or two layers having the
wrong stacking sequence such as AaBbAa/CcBbCc.
This defect is a stacking fault and is found in materials
having the wurtzite structure.[28] For this defect it is
important to notice that there is no change in polarity.

In the case of inversion domain boundaries (IDB),
there is a change of polarity. The regions on both sides
of the boundary plane are related by an inversion. IDBs
have been observed in ZnO ceramics that contain addi-
tives such as $Bi_4Ti_3O_{12}$ and Sb_2O_3. In these materials,
the dopants are believed to allow the formation of an
IDB. Models describing the atomic structure at the IDB
interface have been proposed with only Zn and O atoms
and with the incorporation of impurity atoms.[30,31] But
in all the materials studied that exhibit IDB, impurities
were present and are believed to stabilize the polarity
reversal. Due to the low processing temperatures used
for ZnO thin film growth and the tendency for the
wurtzite structure to allow the formation of stacking
faults and IDB, it is likely that these types of planar de-
fects will be produced during thin film deposition. Con-
cerning wurtzite films, recently a lot of results have been
obtained on the microstructure and defects of GaN films
deposited epitaxially onto various substrates[32–35] due to
the optoelectronic applications associated with the GaN
layer. In all cases dislocations are observed. For some de-
position conditions and substrates, stacking faults and/or
inversion domain boundaries are also present.

Yoshino *et al.*[36] have observed by TEM the inter-
faces ZnO–Au, ZnO–Glass, and ZnO–Al. The inter-
faces were either amorphous or the *c*-axis orientation
begins directly at the substrate as it was the case for the
Au interface. On sapphire single crystal,[36,37] ZnO grows
epitaxially, but some dislocations were probably present.
The focus of these studies was more on interfaces; our
paper presents a detailed study of the microstructure and
defects (close and far from the interface) of ZnO thin
films deposited onto Au coated optical fibers and flat
glass substrates. The ZnO thin films were deposited by
reactive magnetron sputtering without substrate heating.
Low temperature deposition processes, such as the one
used for this work, typically result in ZnO films with
significant 0002 peak broadening and therefore probably
a high density of defects that disrupt the lattice along
the [0001] direction. A few reports on ZnO thin films
have shown that changes in 0002 XRD peak width
can be correlated with changes in electrical and optical
properties.[6,7] Because of the relationship between peak
width and the properties of ZnO thin films, it is of in-
terest to identify the origin of the 0002 peak broadening
and the exact nature of the defects in order to obtain a

better understanding of the microstructural features that
control ZnO thin film properties.

Results from XRD, SEM, and TEM are used to char-
acterize film preferred orientation and grain morphol-
ogy. High resolution transmission electron microscopy
(HRTEM) and lattice image simulations are used to
identify the types of planar defects that occur in ZnO
thin films. The relation between the observed defects
and the 0002 peak broadening is also discussed.

II. EXPERIMENTAL PROCEDURE

Thin films of ZnO were deposited by reactive dc
magnetron sputtering on Cr/Au coated 125 μm diameter
telecommunications optical fiber and glass slides. Before
deposition, the protective polymer coating was removed
from fiber samples, and the fiber surface was cleaned
in sequential baths of dichloromethane and isopropanol.
Acetone and isopropanol were used to clean the flat glass
substrates. The Cr and Au coatings were deposited se-
quentially by thermal evaporation, and the deposited Au
films exhibited a [111] preferred orientation according
to XRD analysis. During Cr/Au deposition, the optical
fibers were rotated at a rate of 2.0 rpm in order to
produce uniform concentric coatings on the fiber surface.
The fibers and the flat glass substrates were coated
simultaneously with a source to substrate distance of
15.5 and 16.5 cm, respectively. Due to the fiber rotation,
the deposition rate and the deposited film thicknesses
on the flat glass substrates were approximately π times
those obtained for the fiber substrates. Deposition rates
of 1 and 10 nm/min were used to deposit thicknesses
of 13 and 130 nm of Cr and Au, respectively, on fiber
substrates.

The ZnO thin films were deposited by reactive dc
magnetron sputtering from a 10 cm diameter Zn metal
target placed 8.5 and 9.5 cm from the fiber and the flat
glass substrates, respectively. A dc power of 250 W was
applied to the target and a mixed Ar/O_2 atmosphere with
a total pressure $P = 1.50$ Pa and oxygen partial pressure
$P_{O_2} = 0.70$ Pa was maintained during deposition. The
fibers were rotated at a rate of 5.6 rpm during the
deposition. Details on the deposition process have been
previously reported.[38]

X-ray diffraction was used to analyze the crystalline
phase formation and preferred orientation of the ZnO
thin films. A 114.6 nm diameter Debye–Scherrer camera
was used to analyze the thin film fiber coatings since
this technique is ideal for analysis of fiber samples and
can provide information about radial textures. A standard
Bragg–Brentano diffractometer was used for analysis of
thin films deposited on flat substrates. Both diffraction
techniques utilized Cu K_α radiation.

Both fracture cross section and surface images of the
deposited films were obtained with a JEOL 6300F scan-

ning electron microscope. Low beam currents were used to obtain secondary electron images without applying additional conductive coatings to the samples.

Cross-section samples of coated fibers and flat substrates were investigated by TEM. Coated fibers were first cut into 2 mm long sections. Approximately five pieces of fiber were then glued between two 2×3 mm^2 silicon wafers using epoxy cement. For the flat substrate, two coated substrates were glued together with the ZnO films facing each other. The "sandwich" structures were then ground to a thickness of approximately 30 μm and then fixed with epoxy to a copper grid. The samples were ion milled by opposing ion beams with an incident angle of 15°, accelerating voltage of 4 kV, and a total beam current of 1 mA. TEM observations were made with a Phillips EM430ST having a spherical aberration coefficient of 1.1 mm. The microscope was operated at 300 kV, resulting in a point-to-point resolution of 0.2 nm. TEM observations were made at different locations of the coatings, but most of the observation concentrated on areas close to the ZnO/Au interface.

III. RESULTS AND DISCUSSION

A. SEM observations

ZnO coatings deposited onto fibers and flat substrates using the same deposition conditions exhibit columnar microstructures. For flat substrates the columns grow perpendicular to the substrate surface plane. On fibers, the columns also grow perpendicular to the substrate surface, resulting in a radial growth direction for the columns. The columnar microstructure of a fiber coating is shown in Fig. 1(a). At the Au/ZnO interface the ZnO columns have a diameter of 100 nm, and this column diameter increases to approximately 400 nm at the surface of the 5 μm thick coating. This increase in column diameter with thickness results in a column divergence angle of approximately 2°. On close inspection of the columns, a fine-scale multilayer morphology is observed as shown in Fig. 1(b). At the bottom of the columns, near the Au/ZnO interface, the layered morphology is perpendicular to the column axis, i.e., the growth direction of the columns. The boundaries of the layers are separated by a distance of 20–30 nm. At the top of the columns the layers become tilted and can even exhibit zigzag or chevron-type structures having mirror symmetry with respect to the column axis.

B. XRD characterization

XRD analysis of coated fibers and flat substrates revealed that the films consisted of phase pure ZnO with the wurtzite structure and that the films exhibit an [0001] preferred orientation or texture perpendicular to the plane of flat substrates and radial with respect to
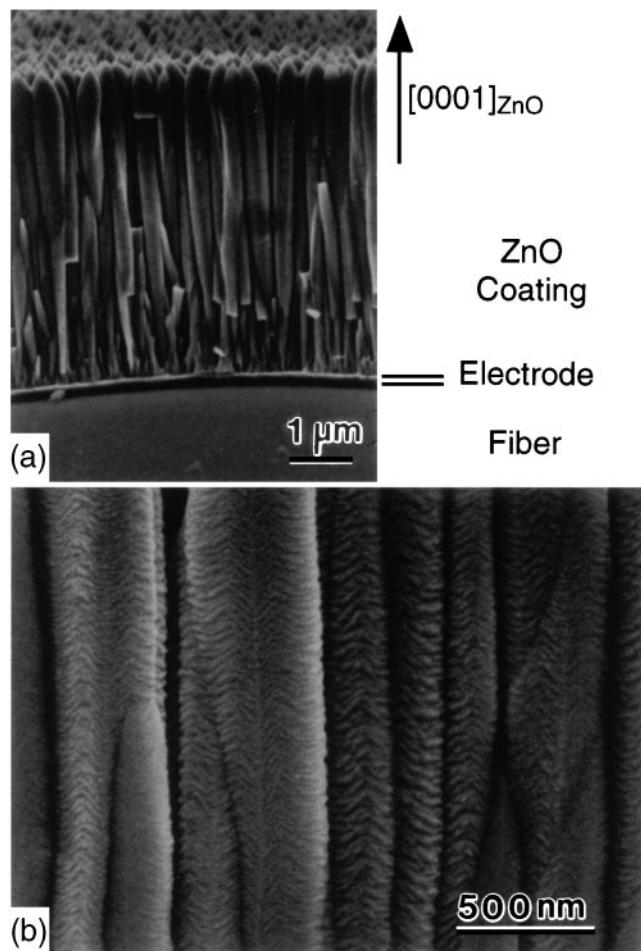

FIG. 1. (a) SEM secondary electron image showing the columnar structure of a ZnO coating deposited onto a Cr/Au coated glass fiber. (b) SEM secondary electron image showing 20–30 nm spacing of multilayer morphology perpendicular to columnar growth direction.

the fiber axis of fiber substrates. The results from both flat and fiber samples confirm that the [0001] preferred orientation lies along the column axis of the columnar ZnO microstructure. The [0001] preferred orientation for flat substrates was determined by the occurrence of high intensity 000l reflections (where l is an integer) and the absence of all other reflections. For fiber samples analyzed with a Debye−Scherrer camera, the [0001] radial preferred orientation could be determined from the high relative intensity of the 000l reflections and the change of the 000l reflections from continuous rings to short arcs on the exposed film.[38]

By comparing the thin film 0002 peak width at half maximum intensity with a ZnO powder pattern, it is apparent that the ZnO coatings on both flat and fiber substrates exhibit significant broadening as shown in Figs. 2 and 3, respectively. Broadening of the diffraction peaks results when imperfections of the crystalline lattice are separated by a distance of less than approximately 100 nm or inhomogeneous strains occur within

the crystal. The distance between lattice imperfections is commonly referred to as "crystallite size" or the coherent crystal length.[27] Powder patterns (solid lines) for comparison with the thin film patterns (dashed lines) were obtained by both diffractometer and Debye−Scherrer camera techniques since there is a significant difference in the instrumental broadening for the two techniques. To a first approximation, it can be assumed that the instrumental peak widths, b, for the diffractometer and Debye−Scherrer camera are the same as the peak widths obtained from the powder patterns since these patterns were obtained from a relatively large grain powder that was calcined to remove lattice defects. The peak
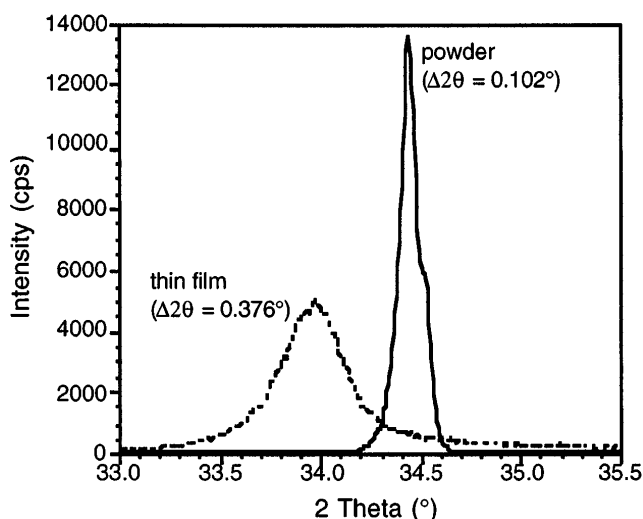

FIG. 2. XRD 0002 reflections obtained from ZnO powder (solid line) and a ZnO thin film deposited onto a flat Cr/Au coated glass substrate (dashed line).
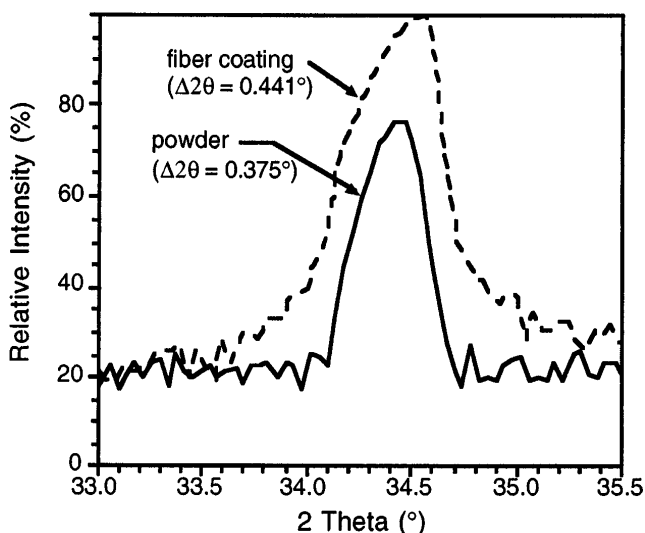

FIG. 3. Debye−Scherrer camera XRD 0002 reflections obtained from ZnO powder (solid line) and a ZnO coating deposited onto a Cr/Au coated glass fiber (dashed line).

width or broadening resulting from imperfections in the crystalline lattice, β (Table I), can be estimated by subtracting b from the measured peak width, B.

Once β is obtained, an estimate of the coherent crystal length, L, can be obtained from the Scherrer formula[27]

$$L = 0.9\lambda/\beta \cos \theta , \qquad (1)$$

where λ is the x-ray radiation wavelength (0.15406 nm for this study) and θ is the Bragg angle of the broadened reflection. It should be noted that the value of the coherence length, L, is an approximation that in particular neglects contributions of nonuniform strain, which very likely also contributes to 0002 peak broadening in the ZnO films. The relative contributions of nonuniform strain and coherent crystal length to the peak width (0.2−0.3°) has not been determined, but the knowledge of L_{0002} will be very useful in determining which defects may explain such a large 0002 peak width.

Peak widths and estimates of coherent crystal length are summarized in Table I for coatings on flat and fiber substrates. A coherent crystal length of $L_{0002} = 35$ nm is calculated from measurements of films deposited on flat substrates. In comparison, the coherent crystal length (Fig. 3) calculated for fiber coatings is 145 nm.

The value for L_{0002} calculated for the fiber coatings is significantly larger than that obtained for films deposited on flat substrates. This difference is believed to result from errors originating with the Debye−Scherrer technique. With Debye−Scherrer measurements, the diameter of the sample and the effective thickness of the sample can influence the measured peak width.[39] The Debye−Scherrer powder pattern was produced from a 200 μm diameter glass capillary filled with powder, and the pattern for the ZnO fiber coating was produced from a 6 μm thick ZnO coating on a 125 μm diameter fiber. Because of the differences between the sample diameters and effective thickness of the ZnO material, a significant error in the determination of β_{0002} is expected when the powder pattern is used to estimate b. The error is due to the fact that b is dependent on sample geometry, which is not exactly the same for powder and coated fiber samples. Evidence for the existence of this error can be seen by comparing the peak widths for the powder and

TABLE I. Peak widths and estimated coherent crystal length for ZnO coatings on flat and fiber substrates.

Substrate	B_{0002} (rad)	b_{0002} (rad)	β_{0002} (rad)	L_{0002} (nm)
Flat	6.56×10^{-3}	1.78×10^{-3}	4.78×10^{-3}	35
Fiber	7.70×10^{-3}	6.54×10^{-3} (powder ref.)	1.16×10^{-3}	145
Fiber	7.70×10^{-3}	3.87×10^{-3} (fiber $1\bar{1}00$ ref.)	3.82×10^{-3}	44

fiber coating 10-10 reflections which are 7.17×10^{-3} and 3.87×10^{-3} rad, respectively. Since the instrumental broadening is always less than the total broadening for a peak, $b_{10\text{-}10} \leqslant B_{10\text{-}10}$ for the coated fiber samples. Since $^{\text{coated fiber}}B_{10\text{-}10} < {}^{\text{powder}}B_{10\text{-}10}$, $^{\text{powder}}B_{10\text{-}10}$ cannot be a good estimate of $b_{10\text{-}10}$ for the coated fiber samples. This suggests that $^{\text{powder}}B_{0002}$ greatly overestimates b_{0002} for coated fibers, therefore, leading to a calculated value of L_{0002} that is too large.

Since the $10\bar{1}0$ reflection is close in angular position to the 0002 reflection, the instrumental broadening for the two peaks will be similar for a diffraction pattern obtained from the same specimen and $B_{10\bar{1}0}$ for the fiber coating can be used as an estimate of b_{0002}. A coherent crystal length of $L_{0002} = 44$ nm is obtained for the fiber coating when $B_{10\text{-}10}$ of the fiber sample is used to estimate the instrumental broadening. Although this calculation eliminates the error introduced by differences in sample geometry, it still results in an overestimate of L_{0002} since broadening of the $10\bar{1}0$ peak due to perturbations of the crystalline lattice are included in the estimate of b. Keeping in mind that there are significant errors for the calculation of L_{0002}, it can still be concluded that the calculated values are similar for flat and coated fiber samples.

It should also be noted that for the films deposited on a flat substrate the position of the 0002 peak is displaced relative to the ZnO powder (Fig. 2). This indicates that the ZnO film has a tensile strain along the [0001] direction. This type of tensile strain has previously been observed for ZnO deposited onto (111) oriented Si at room temperature, and can be attributed to a stress in the thin film.[26] The displacement of the 0002 peak is not observed for the fiber coating, which indicates that there is little or no stress in the fiber coating. The difference in strain between films deposited onto flat and fiber substrates may be related to differences in geometry and/or deposition rate.

C. TEM characterization

Figures 4(a) and 4(b) show dark-field images of ZnO deposited onto flat and fiber substrates, respectively. The structure is clearly columnar, and dark lines are observed within the single-crystal ZnO columns. The dark lines predominately lie in planes normal or close to the normal to the column growth direction. These dark lines can be associated with planar defects as it will be shown with the HRTEM analysis. For a large number of grains, the [0001] direction is nearly parallel with the long axis of the columnar grains, which indicates a [0001] preferred orientation. The grain boundaries that define the columns are normal to the substrate surface, i.e., normal to the fiber axis for fiber coatings and the substrate plane for coatings on flat substrates. For the films deposited onto
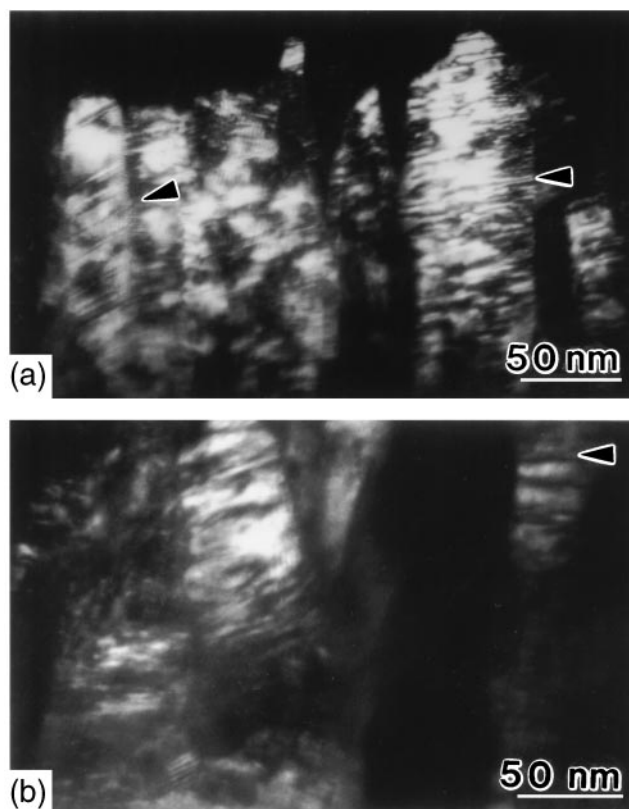

FIG. 4. Dark-field images of ZnO coatings (a) deposited onto a flat substrate and (b) deposited onto a fiber substrate. Note the columnar structure and the presence of dark lines which probably correspond to planar defects (arrowed).

flat substrates, no evidence of amorphous phase was found, but small crystallites were observed close to the substrate interface.[40] The microstructure then transforms to a uniform columnar structure [Fig. 4(a)] for which the column width was about 50–100 nm. This is different from the study of Yoshino *et al.*[36] where it was found that the *c*-axis orientation starts directly at the Au interface. The difference may come from the fact that their films were grown by rf sputtering with a substrate temperature of 250 °C and our substrates were not heated. Therefore, it is believed that the poor crystallinity we observed close to the interface is promoted by the room temperature process. For films deposited onto fibers [Fig. 4(b)], the columns have a diameter of approximately 50 nm near the substrate surface, but the diameter increases to approximately 300 nm close to the surface of the film. The films deposited on flat and fiber substrates exhibit nearly the same microstructure; not only does the column diameter increase in size, but the regularity of the columnar texture also increases on moving away from the Au/ZnO interface toward the ZnO surface. These observations of a columnar microstructure and the [0001] crystal direction which is often parallel with the column axis are consistent with conclusions from XRD and SEM

observations that showed [0001] radial textures for fiber coatings and [0001] texture normal to the substrate plane for deposition onto flat substrates.

HRTEM was used to characterize the defects present within the ZnO columnar grains [Figs. 5(a) and 5(b)]. These images and all other images obtained from both planar and fiber samples indicated that the ZnO films were fully crystallized and no second phases were observed within the grains. However, a large concentration of defects is observed within the grains. Patches of different contrast are also observed. Those are believed to result from slight differences in orientation.

Planar defects lying in the ZnO basal plane, as shown in Figs. 5–7, are observed. Their separation is about 10 nm within both planar films and fiber coatings. In the selected area electron diffraction pattern (Fig. 6) of a single column, some reflections such as the $1\bar{1}00$ are observed to be streaked along [0001]. This streaking of the diffraction pattern is consistent with the presence of planar defects running normal to the [0001] direction. Two different faults were distinguished after careful analysis of the HRTEM images. One type will be referred

FIG. 6. $[11\bar{2}0]$ SAED of a single ZnO grain in a fiber coating. Note the presence of streaked reflections. The 0001 reflection was obtained by double diffraction. The inset (bottom right) represents wurtzite reflections between which streaks along [0001] are present.

FIG. 7. (a) HRTEM image along the $[11\bar{2}0]$ showing a single fault. The image was obtained from a ZnO fiber coating. (b) Schematic of a single stacking fault (type I) viewed along $[11\bar{2}0]$. Only the oxygen atoms (circles) are represented.
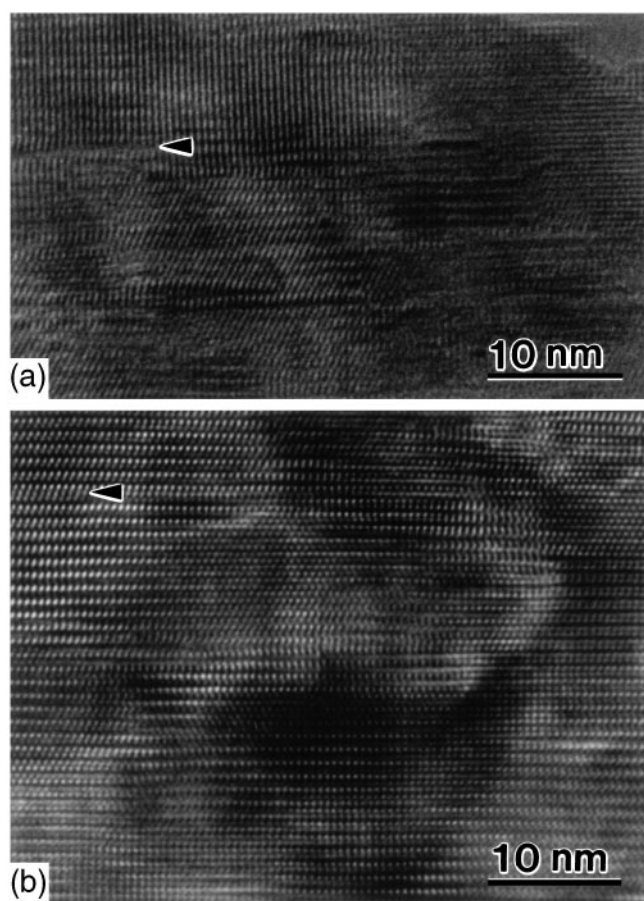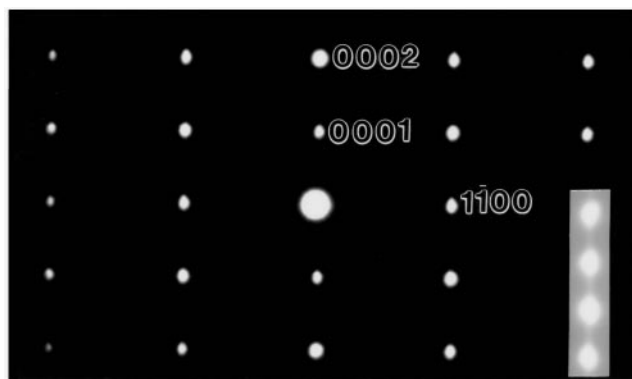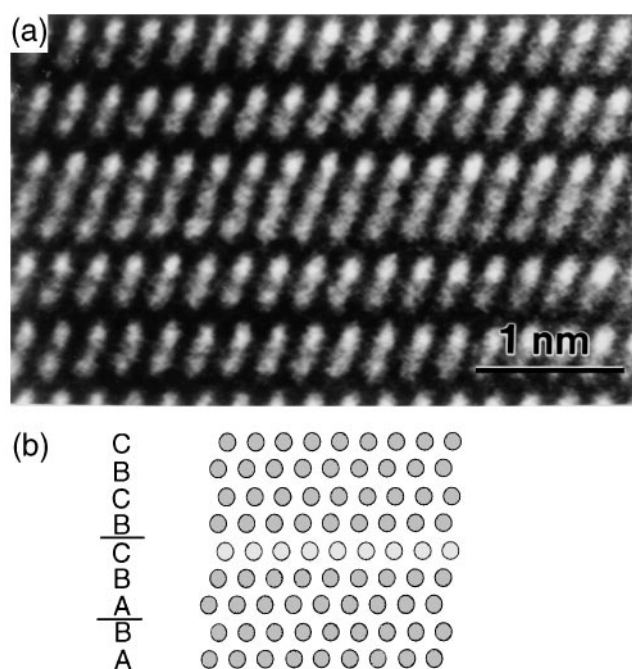

FIG. 5. HRTEM images of single ZnO grains in coatings deposited on (a) flat and (b) fiber substrates. Note the presence of planar defects (arrowed) and regions showing different contrasts.

to as a single fault (Fig. 7). The other observed fault will be referred as a double fault (Fig. 8).

Two kinds of planar defects, IDB or stacking faults (SF), have been reported to occur in ZnO. The most accepted methods for unambiguously determining the nature of a planar defect, i.e., whether it is a SF or an IDB, require the use of thickness fringes, or convergent beam electron diffraction. Unfortunately, the small distance between the faults in the ZnO coatings, 10 nm, and the small grain size (about 100 nm) prevented the use of these analysis methods. For single faults (Fig. 7),
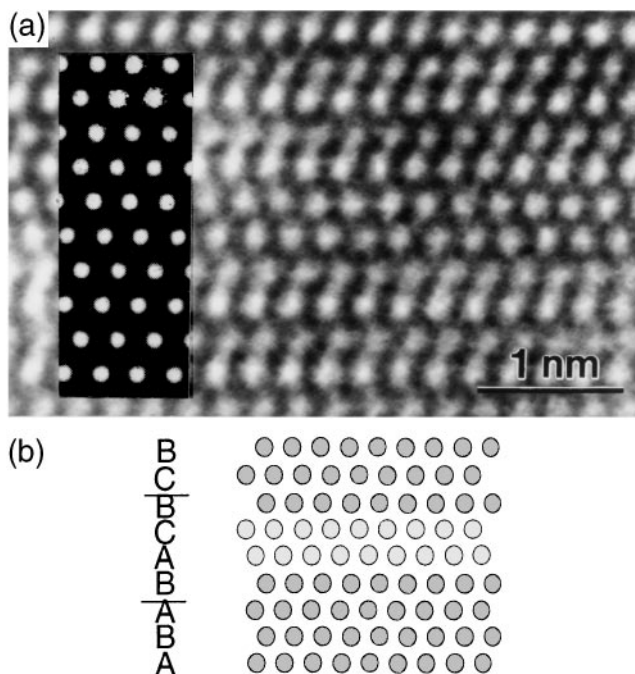
FIG. 8. HRTEM image along the $[11\overline{2}0]$ direction showing a double fault. The image was obtained from a ZnO fiber coating. The inset shows an image simulation of a double stacking (type II) fault obtained from a computer program developed by Stadelmann.[41] Simulation parameters: defocus close to Scherzer: 60 nm and thickness of 6.5 nm. (b) Schematic of a double stacking fault viewed along $[11\overline{2}0]$. Only the oxygen atoms (circles) are represented.

the displacement of the crystalline lattice across the fault plane was measured to be $1/6$ $[2\overline{2}03]$. For double faults (Fig. 8) the displacement across the fault plane was determined to be $1/3[1\overline{1}00]$. The measured displacements across the fault planes are consistent with the occurrence of stacking faults.

Because of the clarity of the image in Fig. 8, the double fault was chosen for simulation. The structure of the double stacking (type II) fault is, for example, AaBbAa[BbAaCcBb]CcBbCcB. It consists of two violations in the stacking sequence. There is no expansion in the [0001] direction, but there is a displacement in the (0001) plane of $1/3[1\overline{1}00]$. The inset of Fig. 8 is the simulated image of a double stacking fault. It can be seen that there is very good agreement between the simulated and experimental images. Some differences are observed outside the vicinity of the planar defect, but these differences are due to a slight misalignment of the $[1\overline{1}20]$ zone axis with respect to the electron beam. The contrast of the IDB structure proposed by McCoy *et al.*[30] and Kim *et al.*[31] was also simulated, but the simulated image did not match the experimental images. Moreover in the proposed models for IDBs in ZnO,[30,31] an apparent displacement in the image along the [0001] direction of about 0.1 nm is present for most of the conditions. This displacement is always observed in the experimental

image of McCoy *et al.*[30] and Kim *et al.*[31] In the proposed IDB models,[30,31] little or no expansion along [0001] was present for the nearly closed packed oxygen lattice, but a displacement was present for the Zn lattice along [0001]. This displacement associated with the Zn lattice is likely to have an effect on the image. The presence of stacking faults is also in agreement with what is reported in the literature. In ZnO ceramics, only stacking faults could be observed when no dopants were present[29] and IDB appeared when dopants were present.[29,30] They suggest that the presence of dopants may be a prerequisite for the formation of IDB. This requirement of dopants for IDB formation may result from the fact that the change of polarity is likely to require a high formation energy, and this energy requirement could be decreased with the presence of foreign species. In our thin film samples, no dopants were introduced and no impurities were found by energy dispersive spectrometry, suggesting that IDBs should not be energetically preferred. In the study of Kim and Goo,[31] a model of an IDB was proposed that did not include any segregants, but in reality their experimental material contained various dopants; therefore, it cannot be excluded that dopants were the main cause of the observed IDBs. In GaN films, which also have the wurtzite structure, IDBs were reported to lie mainly normal to the (0001) plane[34] [e.g., in the $(1\overline{1}00)$] and probably nucleated at the substrate interface. SFs were observed to lie on the (0001) plane.[35] Those results are in agreement with the presence of stacking faults on the (0001) plane in the ZnO films presently studied.

The planar defects are not always located on the (0001) plane but are sometimes observed to step (Fig. 9) or to reside in other planes. For example they can lie on the $\langle 1\overline{1}00\rangle$ or on the $\langle 11\overline{2}0\rangle$ planes instead of the (0001) plane. When a planar defect has only a translation character and does not lie on the basal plane as it is the case for a stacking fault, it has been called a translation domain boundary[32] or a double positioned boundary[35] in other studies.

Dislocations were also observed for the coated fiber and flat substrate samples. Figure 9 shows a lattice image containing a dislocation as well as two other planar defects. The projection of the Burgers vector for the dislocation onto the $(11\overline{2}0)$ plane is $1/2[0001]$. On either side of the dislocation, a stacking fault is present, and the stacking faults exhibit different rigid body displacements of $1/6[2\overline{2}03]$ and $1/6[2\overline{2}00]$, indicating single and double stacking faults, respectively. The interaction between the dislocation and the stacking faults can be expressed in terms of their displacements:

$$d_{\text{SSF}} + b = d_{\text{DSF}}$$

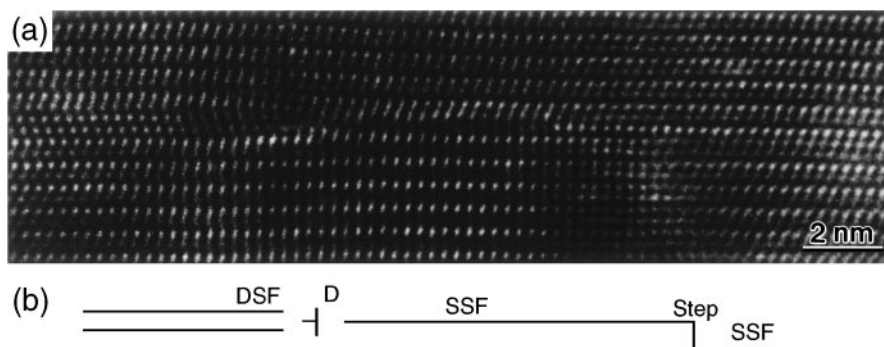(modulo a translation vector of the hexagonal lattice),

(2)

FIG. 9. (a) HRTEM image along the $[11\bar{2}0]$ and (b) a schematic representation showing the interaction between stacking faults and a partial dislocation.

where d_{SSF} is the displacement vector of the single stacking fault, d_{DSF} is the displacement vector of the double stacking fault, and b is the Burgers vector of the dislocation. Using Miller indices, Eq. (2) can be expressed as

$$1/6[2\bar{2}03] + 1/2[0001] = 1/6[2\bar{2}06] = 1/3[1\bar{1}00]$$
$$(\text{modulo } [0001]) . \quad (3)$$

The dislocations within the planar thin films and fiber coatings produce strain. They are often associated with a slight change in contrast and very likely cause a slight change in crystal orientation as in the case for dislocations forming a low-angle grain boundary. Their exact concentration is very high but difficult to estimate since only the dislocations which are closed to an edge geometry and for which the dislocation line is parallel to the axis of observation are easily detected by HRTEM. Their mean separation is estimated to be in the order of 10 nm which corresponds to a density of about 10^{12} cm^{-2}.

D. Discussion

From the observations of the microstructure and lattice defects, it is possible to get a clearer image of the origins for 0002 peak broadening observed in the XRD spectra. As mentioned earlier, possible origins are nonhomogeneous strain and defects which create perturbation of the lattice along [0001] and correspond to a coherence length which was estimated to be about 40 nm in this direction if nonuniform strain is neglected. Those defects include large and low-angle grain boundaries, planar defects in general, and dislocations. The possible effects on the 0002 peak broadening of these different defects are going to be discussed. It has been proposed that grain boundaries are responsible for the 0002 peak broadening.[7] In this study, it was shown that the microstructure is columnar (Figs. 1 and 4); therefore, a limited number of large-angle grain boundaries parallel to the substrate film interface is present, and if large-angle grain boundaries were responsible for the 0002 peak broadening, a coherence length on the order of 1 μm would be expected. Thus, it is very unlikely that the large-angle grain boundaries are responsible for the observed peak width. Low-angle grain boundaries may be considered present since the dislocations which were observed within the columnar grains likely produce regions of materials of slightly different orientations. The interface between two regions may be considered to be similar to a low-angle grain boundary. The effect of dislocations on the 0002 peak broadening will be discussed later. TEM analysis revealed a high density of stacking faults lying on the basal plane. It has been well documented that stacking faults in hexagonal close-packed structures produce only broadening in XRD *hkil* reflections with $h - k = 3n \pm 1$, where h and k are Miller indices and n is an integer value.[42] Since the 0002 reflection does not satisfy this condition, it can be concluded that the stacking faults observed by TEM cannot be the cause of the 0002 peak broadening. The physical reason why stacking faults do not cause broadening of the 0002 peak is because stacking faults do not change the interplanar spacing of the (0002) planes. A high density of dislocations was also observed. Those dislocations introduce changes in (0002) lattice spacing and changes in orientation as it is the case for dislocations composing a low-angle grain boundary and therefore likely contribute significantly to the 0002 peak broadening. The separation between the observed dislocations in lattice images (Fig. 6) and the dimension of the regions showing different contrasts in the lattice images are both approximately 10 nm. This suggests that the crystal coherence length could be 10 nm according to TEM observations, which can be compared to the 35–45 nm "crystallite size" or coherence length calculated from XRD peak broadening. The discrepancy between the 10 nm interspacing determined from TEM observations and $L_{0002} = 35$–45 nm from XRD analysis can be attributed to the fact that the Scherrer formula is

an approximation and that there are significant sources of error in determining the true broadening due to perturbations of the crystalline lattice. If we had considered Gaussian shapes for the XRD 0002 peaks, then $(B_{0002})^2 = (b_{0002})^2 + (\beta_{0002})^2$ and a coherence length of about 25 nm for deposition onto flat substrates and onto fibers would have been found. In addition, the dislocations will also produce nonuniform strain which probably contribute to the 0002 peak width. It should also be noted that the XRD measurement of L_{0002} gives an average measurement for a macroscopic volume of the film, while the TEM observations are limited to projections of a microscopic volume and the determination of the average spacing between the dislocations is associated with a large uncertainty. In ZnO films, nonuniform strain other than the strain associated with dislocations may be present. It may, for example, come from variation in stoichiometry and variation of strain associated with lattice mismatch (between ZnO and the substrate). We have no experimental evidence of stoichiometry variations and nonuniform strain associated with lattice mismatch in our films. It is concluded that the presence of the high concentration of dislocations explains a large 0002 peak width, but contributions of nonuniform strain other than the ones produced by dislocations cannot be completely excluded.

The multilayer structure observed by SEM [Fig. 1(b)] may also be linked to the defect structure observed by TEM. A multilayer structure can be observed by SEM because the sides of the columns exhibit a surface roughness with a periodicity of 20–30 nm. This periodicity is similar to the dislocation and stacking fault spacing of approximately 10 nm, suggesting that the multilayer structure may be associated with these defects. For example, the chevron structure may be related to the planar defects. In some regions, the multilayer structure could correspond to stacking faults; in other regions the planar defects could no more lie in the (0001) plane and correspond to translation domain boundaries.

IV. SUMMARY

ZnO thin films deposited at room temperature onto planar and fiber substrates exhibit columnar microstructures with [0001] texture perpendicular to the substrate surface. For fiber samples, the [0001] texture is in the radial direction due to the curved surface of the fiber. No sign of second phases were observed, but a large number of lattice defects are present. HRTEM analysis revealed a large concentration of partial dislocations and planar defects. Our analysis is in very good agreement with the presence of single (type I) and double stacking faults (type II) for which the displacement is, respectively, $1/6\langle 2\bar{2}03\rangle$ and $1/3\langle 1\bar{1}00\rangle$. The distance between the faults and dislocations is approximately 10 nm. The overall defect configuration gives a mosaic-like structure. Very similar defects are observed for ZnO grown on either fiber or flat substrates, demonstrating that the observed defects are not the result of the geometry of the sample.

REFERENCES

1. F. S. Hickernell, Proc. IEEE **64** (5), 631 (1976).
2. T. Shiosaki and A. Kawabata, Ferroelectrics **42**, 219 (1982).
3. M. Ieda, Y. Suzuoki, M. Nakagawa, and T. Mizutani, IEEE Trans. Electr. Insulat. **25** (3), 599 (1990).
4. F. S. Mahmood, R. D. Gould, A. K. Hassan, and H. M. Salin, Thin Solid Films **270**, 376 (1995).
5. M. Imura, T. Tanaka, M. Homma, and M. Okada, Mater. Trans. **35** (10), 730 (1994).
6. R. G. Heideman, P. V. Lambeck, and J. G. E. Gardeniers, Opt. Mater. **4**, 741 (1995).
7. H. Nanto, T. Minami, S. Shooji, and S. Takata, J. Appl. Phys. **55** (4), 1029 (1984).
8. U. Lampe and J. Müller, Sensors and Actuators **18**, 269 (1989).
9. C. R. Wüthrich, C. A. P. Muller, G. R. Fox, and H. G. Limberger, *Proceedings IEEE, International Conference on Solid-State Sensors and Actuators* (Institute of Electrical and Electronics Engineers, Inc., Piscataway, NJ, 1997), p. 97.
10. G. R. Fox, C. R. Wüthrich, C. A. P. Muller, and N. Setter, Ferroelectrics **201**, 13–22 (1997).
11. G. R. Fox, C. A. P. Muller, N. Setter, D. M. Costantini, N. H. Ky, and H. G. Limberger, J. Vac. Sci. Technol. A **15** (3), 1791 (1997).
12. M. D. Mermelstein, Appl. Opt. **22** (7), 1006 (1983).
13. M. Imai, H. Tanizawa, Y. Ohtsuka, Y. Takase, and A. Odajima, J. Appl. Phys. **60** (6), 1916 (1986).
14. S. Trolier-McKinstry, G. R. Fox, A. Kholkin, C. A. P. Muller, and N. Setter, in *Materials for Smart Systems II,* edited by E. P. George, R. Gotthardt, K. Otsuka, S. Trolier-McKinstry, and M. Wun-Fogle (Mater. Res. Soc. Symp. Proc. **459**, Pittsburgh, PA, 1997), pp. 189–194.
15. F. S. Hickernell, J. Vac. Sci. Technol. A **12** (4), 879 (1975).
16. S. Maniv and A. Zangvil, J. Appl. Phys. **49** (5), 2787 (1978).
17. S. B. Krupanidhi and M. Sayer, J. Appl. Phys. **56** (11), 3308–3317 (1984).
18. F. C. M. Van de Pol, F. R. Blom, and T. J. A. Popma, Thin Solid Films **204**, 349 (1991).
19. F. R. Blom, F. C. M. Van de Pol, G. Bauhuis, and T. J. A. Popma, Thin Solid Films **204**, 365 (1991).
20. T. Shiosaki and A. Kawabata, Ferroelectrics **42**, 219 (1982).

21. F. S. Hickernell, IEEE Ultrason. Symp. Proc. **2**, 785–794 (1980).
22. M. Matsuoka, Y. Hoshi, and M. Naoe, J. Appl. Phys. **63** (6), 2098 (1988).
23. Y. Ito, K. Kushida, H. Kanda, H. Takeuchi, K. Sugawara, and H. Onozato, Ferroelectrics **134**, 325 (1992).
24. K. Tominaga, M. Shirai, and H. Imai, Jpn. J. Appl. Phys. **30** (9B), 2216 (1991).
25. L. Meng and M. P. dos Santos, Thin Solid Films **250**, 26–32 (1994).
26. R. J. Lad, P. D. Funkenbusch, and C. R. Aita, J. Vac. Sci. Technol. **17** (4), 808–811 (1980).
27. H. P. Klug and L. E. Alexander, *X-Ray Diffraction Procedures,* 2nd ed. (John Wiley and Sons, Inc., New York, 1974), pp. 618–708.
28. H. Blank, P. Delavignette, R. Gevers, and S. Amelinckx, Phys. Status Solidi **7**, 747–764 (1964).
29. D. Makovec and M. Trontelj, J. Am. Ceram. Soc. **73** (5), 1202 (1994).
30. M. A. McCoy, R. W. Grimes, and W. E. Lee, J. Mater. Res. **11**, 2009 (1996).
31. J. C. Kim and E. Goo, J. Am. Ceram. Soc. **73** (4), 877 (1990).
32. J-L. Rouvière, M. Arlery, R. Niebuhr, and K. H. Bachem, Inst. Phys. Conf. Ser. **No. 146**, 285 (1995).
33. N-E. Lee, R. C. Powell, Y-W. Kim, and J. E. Greene, J. Vac. Sc. Technol. A **13** (5), 2293 (1995).
34. J-L. Rouvière, M. Arlery, B. Daudin, G. Feuillet, and O. Briot, Mater. Sci. Eng. B **50**, 61 (1997).
35. Y. Xin, P. D. Brown, C. J. Humphreys, T. S. Cheng, and C. T. Foxon, Appl. Phys. Lett. **70**, 1308 (1997).
36. Y. Yoshino, S. Iwasa, H. Aoki, Y. Deguchi, Y. Yamamoto, and K. Ohwada, in *Thin Films–Structure and Morphology,* edited by S. C. Moss, D. Ila, R. C. Cammarata, E. H. Chason, Th. L. Einstein, and E. I. Williams (Mater. Res. Soc. Symp. Proc. **441**, Pittsburgh, PA, 1997), p. 241.
37. H. B. Kang, K. Nakamura, S. H. Lim, and D. Shindo, Jpn. J. Appl. Phys. **37**, 781 (1998).
38. G. R. Fox, N. Setter, and H. G. Limberger, J. Mater. Res. **11**, 2051 (1996).
39. H. P. Klug and L. E. Alexander, *X-Ray Diffraction Procedures,* 2nd ed. (John Wiley and Sons, Inc., New York, 1974), pp. 175–270.
40. L. Sagalowicz, G. R. Fox, M. A. Dubois, C. A. P. Muller, P. Muralt, and N. Setter, J. Eur. Ceram. Soc. (1999, in press).
41. P. A. Stadelmann, Ultramicroscopy **21** (2), 131 (1987).
42. G. B. Mitra and N. C. Halder, Acta Crystallogr. **17**, 817 (1964).